

1 **Coupled Feedbacks on the Northern Hemisphere Midlatitude Jet Response**  
2 **to 4xCO<sub>2</sub>: Changes in Stratospheric Ozone and the Atlantic Meridional**  
3 **Overturning Circulation**

4 Clara Orbe<sup>a,b</sup>, David Rind<sup>a</sup>, Darryn Waugh<sup>c</sup>, Jeffrey Jonas<sup>a,d</sup>, Xiyue Zhang<sup>c</sup>, Gabriel Chiodo<sup>e</sup>,  
5 Larissa Nazarenko<sup>a,d</sup>, and Gavin A. Schmidt<sup>a</sup>

6 <sup>a</sup> *NASA Goddard Institute for Space Studies, New York, NY*

7 <sup>b</sup> *Department of Applied Physics and Applied Mathematics, Columbia University, New York, NY*

8 <sup>c</sup> *Department of Earth and Planetary Sciences, Johns Hopkins University, Baltimore, MD*

9 <sup>d</sup> *Center for Climate Systems Research, Earth Institute, Columbia University, New York, NY*

10 <sup>e</sup> *Institute for Atmospheric and Climate Science, ETH Zurich, Switzerland*

12 ABSTRACT: Ozone, and its response to anthropogenic forcings, provide an important pathway  
13 for the coupling between atmospheric composition and climate. This applies to stratospheric ozone  
14 as well as ozone in the troposphere; in addition to stratospheric ozone's radiative impacts, recent  
15 studies have shown that changes in the ozone layer due to  $4xCO_2$  have a considerable impact on the  
16 Northern Hemisphere (NH) tropospheric circulation, inducing an equatorward shift of the North  
17 Atlantic jet during boreal winter. Here we show that this equatorward jet shift induces a more rapid  
18 weakening of the Atlantic Meridional Overturning Circulation (AMOC), resulting in a poleward  
19 shift of the jet on longer timescales. As such, coupled feedbacks from both stratospheric ozone  
20 and the AMOC result in a two-timescale response of the NH midlatitude jet to abrupt  $4xCO_2$   
21 forcing: a "fast" response (5-20 years) during which the North Atlantic jet shifts equatorward and  
22 a "long" response ( $\sim 100$ -150 years) during which the jet shifts poleward. The latter is driven by  
23 a weakening of the AMOC that develops in response to weaker surface zonal winds, that result  
24 in reduced heat fluxes out of the subpolar gyre, reducing North Atlantic Deep Water formation.  
25 Our results suggest that stratospheric ozone changes in the tropical lower stratosphere can have a  
26 surprisingly powerful effect on the AMOC, independent of other aspects of climate change.

## 27 **1. Introduction**

28 There is large uncertainty in the atmospheric circulation response to increasing greenhouse gases  
29 (e.g., Shepherd (2014)). Although models generally predict a poleward shift of the westerly jet,  
30 the magnitude of this shift is highly uncertain (e.g., Vallis et al. (2015); Grise and Polvani (2014))  
31 as are its underlying drivers (Shaw (2019)). This is especially true in the Northern Hemisphere  
32 (NH), where there are opposing thermodynamic influences, i.e. opposite meridional temperature  
33 gradient responses at the surface versus the upper troposphere (Shaw et al. (2016)). Thus, while  
34 enhanced warming in the lower polar troposphere relative to the lower tropical troposphere (i.e.,  
35 Arctic amplification) contributes to reduced meridional temperature gradients, increases in upper  
36 tropospheric tropical warming contribute to enhanced temperature gradients aloft (Butler et al.  
37 (2010); Yuval and Kaspi (2020)) and it is not clear how these competing processes affect the zonal  
38 mean jet.

39 Many processes have been shown to influence the response of meridional temperature gradients  
40 to increased CO<sub>2</sub>, including polar amplification (see Smith et al. (2019) and references therein)  
41 and cloud feedbacks (e.g., Ceppi and Hartmann (2015); Voigt and Shaw (2015)). By comparison,  
42 composition feedbacks associated with the ozone response to CO<sub>2</sub> have been less well examined  
43 although stratospheric ozone changes have been identified as an important pathway coupling  
44 composition to climate (Isaksen et al. (2009)). In particular, the stratospheric ozone response to  
45 4xCO<sub>2</sub> consists of robust decreases in the tropical lower stratosphere (LS), increases in the tropical  
46 upper stratosphere and increases over high latitudes (Chiodo et al. (2018)). While the exact details  
47 of these changes are model dependent, especially over high latitudes, the general pattern is very  
48 consistent among models (Nowack et al. (2015), Chiodo et al. (2018), Chiodo and Polvani (2019)  
49 (hereafter CP2019)).

50 This pattern of reduced (increased) ozone over the tropical lower (high latitude) LS in response  
51 to 4xCO<sub>2</sub> has immediate implications for temperature gradients in the stratosphere by cooling the  
52 tropics and warming high latitudes (Nowack et al. (2015); Chiodo et al. (2018)). As CP2019  
53 showed, these changes in temperature gradients drive an anomalous equatorward shift of the  
54 midlatitude jet, not only in the Southern Hemisphere (SH), but also in the Northern Hemisphere  
55 (NH), where anomalies extend down into the lower troposphere and are concentrated over the  
56 Atlantic, resembling the negative phase of the North Atlantic Oscillation (NAO).

57 A more recent study by Zhang et al. (Submitted), that considered two models that differed only in  
58 their representation of interactive chemistry, also showed that changes in composition can impact  
59 the sign of the NH midlatitude jet response to increased CO<sub>2</sub>. However, in contrast to CP2019,  
60 the long-term impact of this compositional feedback was a *poleward*, not equatorward, shift in the  
61 North Atlantic jet. Though not investigated in detail, this poleward shift of the jet was linked to  
62 changes in the ocean circulation, which were not examined in CP2019. More precisely, Zhang et al.  
63 (Submitted) noted that the AMOC exhibited a stronger decline in interactive simulations in which  
64 trace gases and aerosols were allowed to respond to increased CO<sub>2</sub>, relative to non-interactive  
65 versions. Indeed, recent studies have highlighted the large influence that changes in the AMOC  
66 exert on the response of the NH midlatitude jet to increased CO<sub>2</sub> (Gervais et al. (2019)), with  
67 models featuring a larger AMOC decline also tending to produce a stronger poleward jet shift  
68 (Bellomo et al. (2021); Liu et al. (2020); Orbe et al. (Under Review)).

69 The results from Zhang et al. (Submitted) suggest that composition feedbacks on the NH midlat-  
70 itude jet may depend on the response of the ocean circulation. However, that study did not examine  
71 the mechanism underlying the stronger AMOC response in the interactive chemistry simulations  
72 nor did it isolate the role of ozone from influences due to other trace gases and aerosols. To this end,  
73 here we hypothesize that the ozone-induced negative NAO wind anomalies reported in CP2019  
74 provide a potential pathway through which stratospheric ozone changes can influence the AMOC.  
75 Variations in the jet – namely those resembling the NAO – have long been shown to influence  
76 variability of the AMOC through changes in wind stress (Marshall et al. (2001); Zhai and Marshall  
77 (2014)). Modified air-sea fluxes of heat, water and momentum associated with variations in the  
78 NAO alter vertical and horizontal density gradients in the subpolar gyre, inducing changes in deep  
79 water formation and the AMOC (e.g., Visbeck et al. (1998); Delworth and Dixon (2000)). This  
80 pathway via the NAO has been used to demonstrate how sudden stratospheric warmings influence  
81 the variability of heat flux anomalies into the ocean and ocean mixed layer depths in the North  
82 Atlantic (O’Callaghan and Mitchell (2014)) as well as the strength of the AMOC itself (Reichler  
83 et al. (2012)).

84 We begin by showing results from non-interactive and fully interactive chemistry global warming  
85 experiments produced with the new high-top coupled atmosphere ocean version of the NASA  
86 Goddard Institute for Space Studies (GISS) climate model that were submitted to the Coupled



87 Model Intercomparison Project Phase 6 (CMIP6) (Eyring et al. (2016)). We then show that the  
88 AMOC response in the interactive simulations is largely associated with changes in stratospheric  
89 ozone, not aerosols, using new experiments in which the stratospheric ozone response to  $4\times\text{CO}_2$   
90 is isolated from changes in other trace gases and aerosols. In particular, we show that our model  
91 captures the ozone-induced negative NAO-like pattern first reported in CP2019; in addition, we  
92 also find that ozone-driven changes in surface friction speed further weakens the AMOC, resulting  
93 in a long-term poleward shift of the NH jet. As a result, we show that both stratospheric ozone  
94 changes and the AMOC influence the NH jet on distinct “fast” and “long” timescales (and in  
95 the opposite sense), comprising a coupled atmosphere-ocean feedback on the NH midlatitude jet  
96 response to increased  $\text{CO}_2$ . While the former “fast” feedback was documented in CP2019, the  
97 latter has, to the best of knowledge, not been reported in previous studies.

98 It is important to note that previous studies have long shown that interactive atmospheric compo-  
99 sition can strongly influence the AMOC, placing an almost exclusive focus on the role of aerosols  
100 Booth et al. (2012); Cowan and Cai (2013); Swingedouw et al. (2015). More recently, Rind et al.  
101 (2018) also identified a larger sensitivity of the AMOC response to global warming using an in-  
102 teractive configuration of the CMIP5 version of the GISS climate model (GISS-E2-R), compared  
103 to a non-interactive version. In that study, multicentennial cessations of the AMOC were found to  
104 occur in simulations in which natural aerosols (primarily sea salt) were allowed to locally cool sea  
105 surface temperatures through their influence on cloud optical thickness; these cooler SSTs were  
106 then linked to reduced evaporation relative to precipitation, resulting in positive surface freshwater  
107 forcing and reduced NADW production. As in Rind et al. (2018) we also show that compositional  
108 feedbacks play an important role on the response of the AMOC to  $\text{CO}_2$  through their influence  
109 on surface fluxes and surface temperatures. However, the mechanism proposed here only invokes  
110 changes in stratospheric ozone, not aerosols.

111 We begin by discussing methods in Section 2 and present key results and conclusions in Sections  
112 3 and 4, respectively.

## 113 2. Methods

### 114 *a. Model and Configurations*

115 Here we use the NASA Goddard Institute for Space Studies (GISS) “Middle Atmosphere (MA)”  
116 Model E2.2 (Rind et al. (2020); Orbe et al. (2020)). E2.2 consists of 102 vertical levels spanning  
117 the surface up to 0.002 hPa and is run at a horizontal resolution of 2 degrees by 2.5 degrees.  
118 Orographic and non-orographic gravity wave drag is parameterized following Lindzen (1987) and  
119 Rind et al. (1988), producing in E2.2 a quasibiennial oscillation (QBO) that compares well with  
120 observations as well as improved stratospheric polar vortex variability (Ayarzagüena et al. (2020);  
121 Rind et al. (2020)). Among the different model versions discussed in Rind et al. (2020) here we  
122 focus on the “Altered-Physics” (-AP) Version (E2.2-AP) because this is the configuration that was  
123 submitted CMIP6 and presented in recent studies (Ayarzagüena et al. (2020); DallaSanta et al.  
124 (2021a,b)).

125 We begin by showing the results reported in Zhang et al. (Submitted) using both “Non-  
126 INTERactive” (NINT) (Table 1, row 1-3) and fully interactive OMA (“One-Moment Aerosols”;  
127 Bauer et al. (2020)) configurations (Table 1, row 4-6). In the NINT configuration (denoted in  
128 CMIP6 as “physics version 1” on the Earth System Grid Federation (ESFG; <https://esgf.llnl.gov>))  
129 all trace gases and aerosols are set to preindustrial values. Hence, in the 2- and 4xCO<sub>2</sub> NINT runs  
130 neither ozone nor other trace gases (besides water vapor) change in response to increased CO<sub>2</sub>. By  
131 comparison, the OMA 2- and 4xCO<sub>2</sub> runs (denoted in CMIP6 as “physics version 3” on ESGF)  
132 capture the full nonlinear ozone response to CO<sub>2</sub>, as well as composition feedbacks associated with  
133 other trace gases and aerosols.

134 In order to isolate the role of ozone feedbacks on the circulations, we then use a linearized ozone  
135 (LINOZ) configuration (Table 1, row 7-8). In LINOZ (McLinden et al. (2000)) the ozone field is  
136 calculated interactively by Taylor expanding the equation of state around present-day (2000–2010)  
137 values such that the ozone tendency is, to first-order, parameterized as a function of the local ozone  
138 mixing ratio, temperature, and overhead column ozone. Tropospheric ozone is calculated using  
139 monthly mean ozone production and loss rates archived from GEOS-CHEM (Rind et al. (2014)).  
140 In contrast to NINT, therefore, the LINOZ ensemble captures the influence of the ozone response  
141 to CO<sub>2</sub> on the large-scale circulation. Unlike OMA, however, it is much more computationally

146 TABLE 1. The Model E2.2 experiments presented in this study, including preindustrial control, abrupt 2xCO<sub>2</sub>  
 147 and abrupt 4xCO<sub>2</sub> simulations using both NINT (rows 1-3) and OMA (rows 4-6) configurations. Four NINT  
 148 abrupt 4xCO<sub>2</sub> ensemble members are included (row 3) in order to compare with a four member 4xCO<sub>2</sub> ensemble  
 149 produced using the LINOZ configuration (row 8). The 4xCO<sub>2</sub> ensemble mean LINOZ ozone response is also used  
 150 to force four AMIP preindustrial experiments (row 9) in which all forcings other than ozone are set to preindustrial  
 151 values. A LINOZ preindustrial control simulation (row 7) is also examined. All coupled simulations are run  
 152 using the the GISS Ocean v1 (GO1) (i.e., “-G” in CMIP6 notation).

Configuration	Ozone	CO <sub>2</sub>	Ensemble Size	SSTs and SICs
NINT	Preindustrial	Preindustrial	1	coupled (-G ocean)
NINT	Preindustrial	2xCO <sub>2</sub>	1	coupled (-G ocean)
NINT	Preindustrial	4xCO <sub>2</sub>	4	coupled (-G ocean)
OMA	Preindustrial	Preindustrial	1	coupled (-G ocean)
OMA	2xCO <sub>2</sub>	2xCO <sub>2</sub>	1	coupled (-G ocean)
OMA	4xCO <sub>2</sub>	4xCO <sub>2</sub>	1	coupled (-G ocean)
LINOZ	Preindustrial	Preindustrial	1	coupled (-G ocean)
LINOZ	4xCO <sub>2</sub>	4xCO <sub>2</sub>	4	coupled (-G ocean)
NINT	LINOZ 4xCO <sub>2</sub>	Preindustrial	4	AMIP (Preindustrial SSTs and SICs)

142 efficient to run and isolates the ozone feedback from feedbacks related to other trace gases and  
 143 aerosols. DallaSanta et al. (2021a) previously showed that the LINOZ ozone parameterization  
 144 reproduces well the vertical structure and seasonal cycle of stratospheric ozone obtained from the  
 145 fully interactive OMA configuration (see their Figure 1).

### 153 *b. Experiments*

154 For the different model configurations (NINT, OMA, LINOZ) we perform 150-year-long abrupt  
 155 2- and 4xCO<sub>2</sub> experiments, in which CO<sub>2</sub> values are abruptly doubled and quadrupled relative  
 156 to preindustrial values. For each model configuration, these experiments are branched from  
 157 a corresponding preindustrial control simulation. For NINT and LINOZ four-member 4xCO<sub>2</sub>  
 158 ensembles are run in order to assess the robustness of any ozone feedbacks. These experiments are  
 159 all conducted using the atmosphere-ocean version of E2.2-AP that is coupled to the GISS Ocean  
 160 v1 (GO1) (i.e., “-G” in CMIP6 notation, hereafter simply E2.2-G). For coupled atmosphere-ocean  
 161 configurations in which (four-member) ensembles are run, different ensemble members are chosen

162 from different initial ocean states spaced 20 years apart in the corresponding preindustrial control  
163 simulation.

164 In addition to the coupled atmosphere-ocean experiments, we also present results from a four-  
165 member ensemble of 60-year-long atmosphere-only AMIP experiments in which sea surface tem-  
166 peratures (SSTs) and sea ice concentrations (SICs) are fixed to preindustrial values, but the monthly  
167 mean time-evolving ensemble mean ozone response from the coupled LINOZ 4xCO<sub>2</sub> experiments  
168 is prescribed (Table 1, row 9). This allows us to quantify the impact of the ozone feedback  
169 represented in LINOZ on the large-scale circulation, absent any contributions from changes in  
170 background CO<sub>2</sub>, sea ice concentrations or sea surface temperatures.

### 171 *c. Analysis*

#### 172 1) TIMESCALES

173 When examining the midlatitude jet response to increased CO<sub>2</sub> we account for the fact that  
174 extratropical circulation changes consist of distinct “fast” and “slow” responses (Ceppi et al. (2018),  
175 hereafter CZS2018). More precisely, CZS2018 show that most of the shift of the midlatitude jets  
176 occurs within 5-10 years of a steplike (abrupt) CO<sub>2</sub> forcing, with little shifts occurring during a  
177 slower response over which SSTs change over subsequent decades. In contrast to the Southern  
178 Hemisphere, zonal asymmetries play an important role in the Northern Hemisphere, where the  
179 influence of local patterns in sea surface temperature change can result in oppositely signed jet  
180 shifts on “slow” timescales. Given this potential for compensating jet shifts on distinct timescales,  
181 we therefore decompose the CO<sub>2</sub> circulation response into “fast” and “long” timescale responses.

182 More precisely, to account for the large internal variability in our runs, perhaps related to a  
183 somewhat larger ENSO amplitude in our model compared to observations (Rind et al. (2020)),  
184 we modify the original approach used in CZS2018 to define our “fast” response as the difference  
185 between the ensemble mean 4xCO<sub>2</sub> response, averaged over years 5-20 (as opposed to years 5-10),  
186 and the corresponding preindustrial control simulation. In addition, instead of focusing on the  
187 “slow” response, defined in CZS2018 as the difference between averages over years 120-140 and  
188 years 5-10, here we examine the “long” response, defined as the difference between the ensemble  
189 mean 4xCO<sub>2</sub> response, averaged over years 100-150, and the preindustrial control simulation. This  
190 approach is more consistent with what was used in Zhang et al. (Submitted) and CP2019, with

191 which we directly compare our results throughout. Note that in response to an abrupt quadrupling  
192 of CO<sub>2</sub> the NINT model configuration produces global mean surface temperature “fast” and “long”  
193 responses of ~2.9°C and ~3.9°C, respectively. Statistical significance of all changes are assessed  
194 relative to the interannual variability in the corresponding preindustrial control simulation for each  
195 configuration (Table 1, rows 1,4,7).

## 196 2) ANALYSIS FIELDS

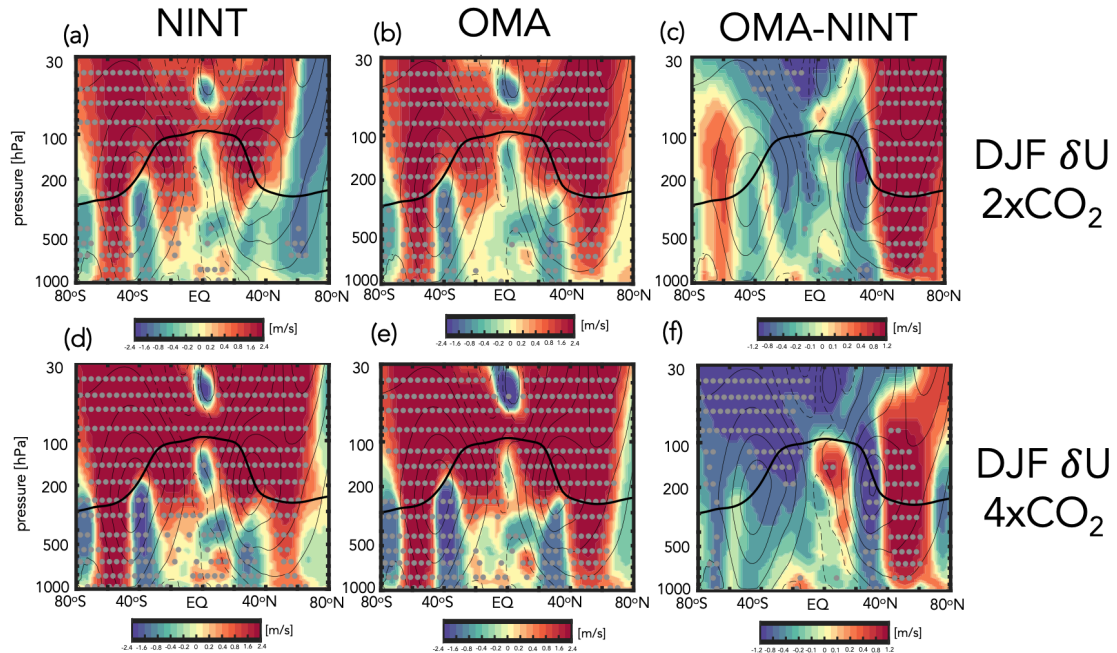
197 In addition to the atmospheric variables examined in CP2019 (i.e., zonal mean wind, zonal mean  
198 temperature, surface temperature, 850 hPa zonal wind) we examine ocean variables relevant to  
199 understanding the evolution of the AMOC and its coupling to the atmosphere. In particular, in  
200 addition to examining the surface mixed layer depths we also examine sea surface temperatures,  
201 surface friction speed, horizontal ocean heat and salinity transports as well as the net heat fluxes  
202 which, together with the net freshwater fluxes,  $F$  (inferred from precipitation minus evaporation  
203 (P-E)), provide information about the surface buoyancy forcing (Large and Yeager (2009)). In our  
204 simulations, the preindustrial climatological buoyancy forcing over the North Atlantic is dominated  
205 by the net heat fluxes ( $Q = Q_H + Q_E + Q_S + Q_L$ ), which are defined to be positive into the ocean  
206 (Appendix Figure 1, left). These are further partitioned into their respective latent heat ( $Q_E$ ) and  
207 sensible heat ( $Q_H$ ) contributions as we find that the net solar ( $Q_S$ ) and longwave ( $Q_L$ ) flux radiative  
208 contributions are negligible over the North Atlantic region (Appendix Figure 1, right).

209 Given our interest in the Northern Hemisphere we focus primarily on December-January-  
210 February (DJF). The ocean heat transport changes in our simulations are also most pronounced  
211 during DJF, consistent with the analyses presented in Romanou et al. (Under Review) and Orbe  
212 et al. (Under Review).

## 213 3. Results

### 214 a. Abrupt 2xCO<sub>2</sub> and 4xCO<sub>2</sub> Zonal Mean Wind Response: OMA versus NINT

215 Before focusing on ozone feedbacks, we first review the OMA versus NINT differences in NH  
216 jet behavior that were presented in Zhang et al. (Submitted) (Figure 1). In the stratosphere the  
217 zonally averaged DJF wind response to 2- and 4xCO<sub>2</sub> features an acceleration at nearly all latitudes,  
218 consistent with amplified warming in the tropical upper troposphere (Shaw (2019)) and increased

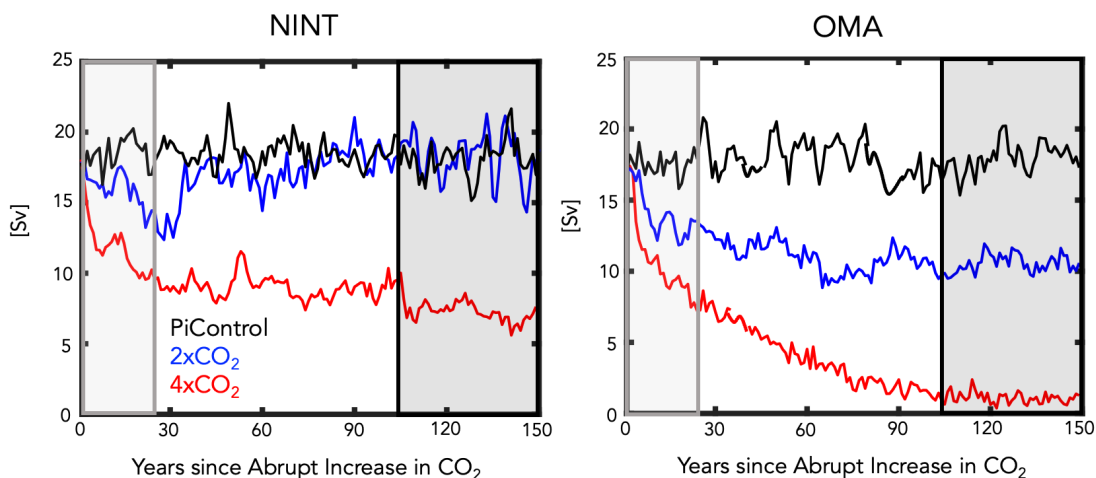


222 FIG. 1. Colors show the December-January-February (DJF) response of the zonal mean zonal winds,  $U$ , to an  
 223 abrupt doubling (top) and quadrupling (bottom) of  $\text{CO}_2$ , averaged over years 100-150. Results are shown for  
 224 the “Non-INTERactive” (NINT) (a,d) and fully interactive OMA (“One-Moment Aerosols”) configurations (b,e),  
 225 where one ensemble member has been used for each forcing scenario. The OMA - NINT differences are also  
 226 shown (c,f). Black contours denote climatological mean DJF  $U$  values (contour interval: 8 m/s). Stippled regions  
 227 are statistically significant and the black thick line shows the climatological mean tropopause in the preindustrial  
 228 control NINT simulation. Note that all colorbar bounds are consistent with those use in Chiodo and Polvani  
 229 (2019) in order to facilitate comparisons with that study.

219 cooling of the stratosphere with height (Garcia and Randel (2008)). Similar wind responses emerge  
 220 in both the NINT and OMA configurations, except over northern high latitudes at  $2\times\text{CO}_2$ , where  
 221 the strengthened zonal winds in NINT are not statistically significant.

230 In the troposphere, however, there are noticeable differences between the OMA and NINT  
 231 simulations. In particular, the NH midlatitude jet features a much stronger poleward shift in OMA,  
 232 compared to NINT (Figures 3 and 6 in Zhang et al. (Submitted)). As discussed in that study, the  
 233 stronger response in OMA results in enhanced eddy mixing along isentropes on the poleward flank  
 234 of the NH jet, resulting in increased transport of tracers from the northern midlatitude surface to  
 235 the Arctic (not shown). This difference between OMA and NINT occurs at both 2- and at  $4\times\text{CO}_2$ ,

## Annual Mean AMOC Response at 48°N



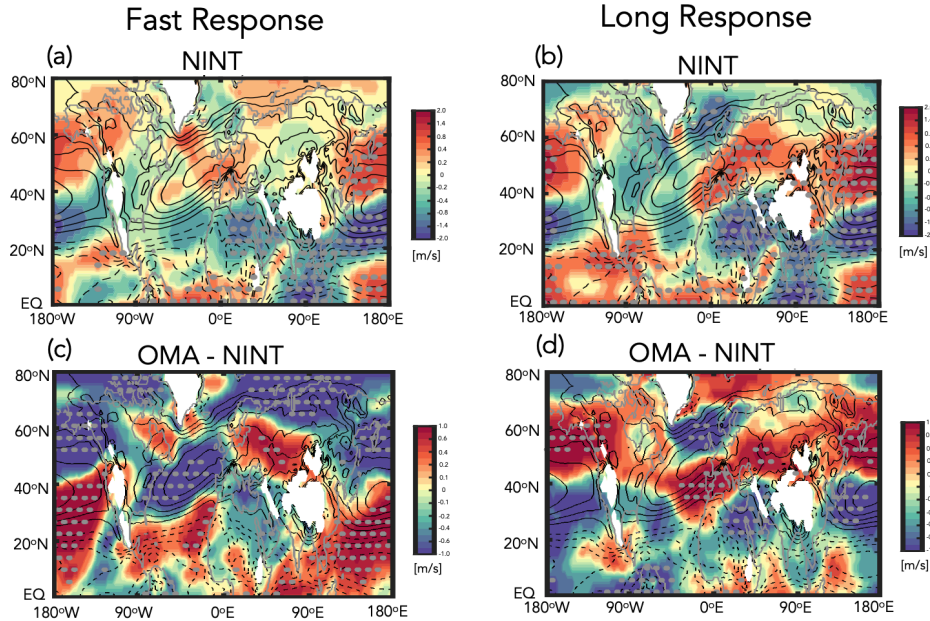
248 FIG. 2. Changes in the annual mean maximum overturning stream function in the Atlantic ocean, evaluated at  
 249 48°N, for the preindustrial control (black), abrupt 2xCO<sub>2</sub> (blue) and abrupt 4xCO<sub>2</sub> (red) simulations. Results for  
 250 the NINT (left) and OMA (right) configurations are shown. Light grey and black shaded boxes denote the “fast”  
 251 and “long” timescale response averaging periods.

236 resulting in a nonlinearity in the jet (and tracer transport) response in NINT that is not present in  
 237 the OMA simulations. In the SH, by comparison, the differences between OMA and NINT are  
 238 much smaller and not statistically significant.

239 Zhang et al. (Submitted) showed that the nonlinearity in NH jet behavior evident in the “long”  
 240 response in the NINT model configuration was related to a nonlinear AMOC response to CO<sub>2</sub>  
 241 forcing (Figure 2). That is, despite an initial weakening, in response to 2xCO<sub>2</sub>, the AMOC  
 242 eventually recovers in the NINT 2xCO<sub>2</sub> simulation to preindustrial values, in contrast to the  
 243 response to 4xCO<sub>2</sub> in which the AMOC is about 10 SV weaker than the preindustrial control (black  
 244 boxes). This results in a so-called “AMOC nonlinearity” of ~-5SV in the NINT configuration.  
 245 By comparison, in the OMA configuration, the AMOC weakens by ~7 and ~17 SV in the 2- and  
 246 4xCO<sub>2</sub> simulations, respectively, representing only a very weak nonlinearity in the AMOC (of  
 247 ~1.5 SV).

252 As it is difficult to meaningfully interpret the zonal mean wind response in the NH, where there  
 253 are large zonal variations in the midlatitude jet (Simpson et al. (2014)), we next compare the 850  
 254 hPa zonal wind changes between the NINT and OMA 4xCO<sub>2</sub> simulations, further distinguishing

## DJF 4xCO<sub>2</sub> $\delta U$ at 850 hPa



265 FIG. 3. Colors show the 4xCO<sub>2</sub> (four member) ensemble mean change in the DJF 850 hPa zonal winds for the  
 266 NINT configuration, decomposed into “fast” (i.e. years 5-20) (a) and “long” (i.e. years 100-150) (b) responses.  
 267 The OMA - NINT fast and long differences are shown in (c) and (d), respectively. Note that one ensemble  
 268 member is used in displaying the OMA - NINT differences (same as used in Figure 1). Black contours denote  
 269 climatological mean DJF values (U contour interval: 2 m/s) and stippled regions are statistically significant.

255 between “fast” and “long” responses (Figure 3). We begin with the NINT equilibrated or “long”  
 256 response (i.e. years 100-150), which consists of a poleward jet shift over the Pacific basin and  
 257 an acceleration and eastward extension of the jet over the Atlantic (Fig. 3b). This pattern is  
 258 amplified in the OMA run (Fig. 3d), in which both the strengthening of the jet over the Atlantic  
 259 and its poleward shift over the Pacific are more pronounced. This wind response in OMA, relative  
 260 to NINT, is consistent with the jet differences identified in Orbe et al. (Under Review) between  
 261 two non-interactive simulations of the GISS low-top climate model in which only the AMOC  
 262 strength differed. This suggests that the jet differences between OMA and NINT on these longer  
 263 timescales are primarily driven by differences in the AMOC response, as concluded in Zhang et al.  
 264 (Submitted).

270 Figure 2 (grey boxes) highlights how the AMOC differences between OMA and NINT noted in  
 271 Zhang et al. (Submitted) arise very early in the simulations (within the first 20 years). Over these



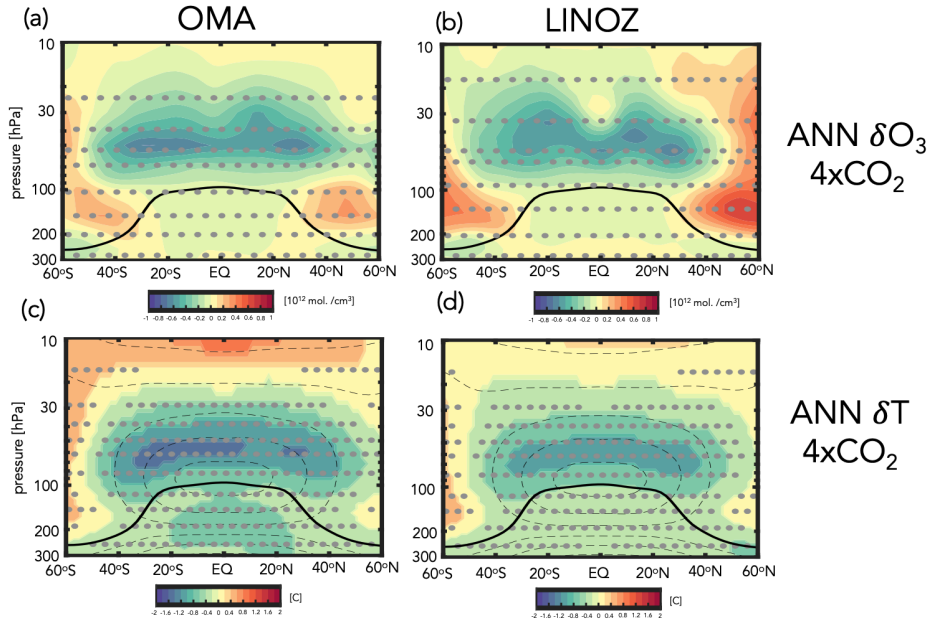
272 years – which comprise the “fast” response – the impact of interactive chemistry on the zonal wind  
273 changes is very different (Fig. 3a,c). In particular, over the Atlantic, interactive composition results  
274 in a strong weakening over the jet core and an acceleration on the equatorward flank of the jet (Fig.  
275 3c). The jet response is also very different over the Pacific, where the jet shifts equatorward, not  
276 poleward as in the NINT simulation (Fig. 3a).

277 This fast composition feedback that occurs over years 5-20 is consistent with the results from  
278 CP2019, who showed that the ozone response to 4xCO<sub>2</sub> induces a weakening of the North Atlantic  
279 jet and a strengthening on its equatorward flank (see their Figure 6). This response is reminiscent  
280 of the negative phase of the NAO which previous studies have shown can result in a weaker  
281 AMOC (Delworth and Zeng (2016)). In CP2019, however, this response is realized through  
282 changes in stratospheric ozone alone, whereas in OMA all trace gases and aerosols are responding.  
283 Furthermore, the significance of this rapid response with only one ensemble member is uncertain,  
284 particularly during the first 5-20 years when the signal is confounded by large internal variability.  
285 To this end, next we present results from the larger (4-member) LINOZ ensemble to examine  
286 whether the fast response in the NH jet is related to stratospheric ozone changes.

### 287 *b. Abrupt 4xCO<sub>2</sub> Stratospheric Ozone and Temperature Responses: OMA versus LINOZ*

288 Before examining the circulation response in the LINOZ ensemble, we first compare the annually  
289 averaged ensemble mean LINOZ 4xCO<sub>2</sub> ozone response with that from the OMA simulation (Figure  
290 4). The amplitude and pattern of the ozone response in the LINOZ ensemble (Fig. 4b) is generally  
291 very similar to the ozone response in the OMA simulation (Fig. 4a). In both configurations the  
292 pattern of the 4xCO<sub>2</sub> changes reflects a decrease in tropical LS ozone, associated with enhanced  
293 tropical upwelling (Garcia and Randel (2008)), and enhanced concentrations over high latitudes.  
294 Over all latitudes the ozone changes are statistically significant, relative to interannual variability  
295 in the preindustrial control simulation.

302 Over northern high latitudes there are some differences in the mid-to-lower stratosphere (~30-  
303 100 hPa) between LINOZ and OMA, generally consistent with Chiodo et al. (2018), who found  
304 that in this region the ozone response to CO<sub>2</sub> is somewhat more model dependent. Furthermore,  
305 both simulations feature small changes in the troposphere. Overall, therefore, the LINOZ scheme  
306 captures the gross characteristics of the ozone abrupt 4xCO<sub>2</sub> response expected from previous



296 FIG. 4. Colors show the annual averaged change in ozone number density (top) and temperature (bottom)  
 297 in response to  $4xCO_2$ . Results for OMA (left) and LINOZ (right) are shown, averaged over years 5-20. One  
 298 simulation is shown for OMA and the four-member ensemble mean response is shown for LINOZ. Black  
 299 contours in the bottom panels show climatological mean temperatures (contour interval: 10 C). Stippled regions  
 300 are statistically significant and the black thick line shows the climatological mean tropopause in the preindustrial  
 301 control NINT simulation.

307 studies. Note that this ozone response occurs in both simulations within the 5-20 years that  
 308 comprise the “fast” response timescale, although full equilibration at high latitudes does take  
 309 somewhat longer (not shown).

310 In response to the ozone changes to  $4xCO_2$  both the OMA simulation and LINOZ ensemble  
 311 produce cooling in the tropical lower stratosphere and warming over high latitudes (Fig. 4c,d). The  
 312 amplitude of the cooling is  $\sim 3K$  in the tropical lower stratosphere, and is more-or-less collocated  
 313 with the region of largest ozone decreases. Further analysis of the temperature tendencies reveals  
 314 that in our model the cooler temperatures in the tropics ( $20^\circ S-20^\circ N$ ) and high latitudes ( $> 40^\circ N$ )  
 315 are respectively associated with reduced and increased radiative heating, primarily in the shortwave  
 316 component (not shown). Dynamically, comparisons of the  $4xCO_2$  changes in the residual mean  
 317 stream function show a weaker response in LINOZ, relative to NINT (not shown). This ozone  
 318 feedback on the Brewer-Dobson circulation, first identified in DallaSanta et al. (2021a), contributes

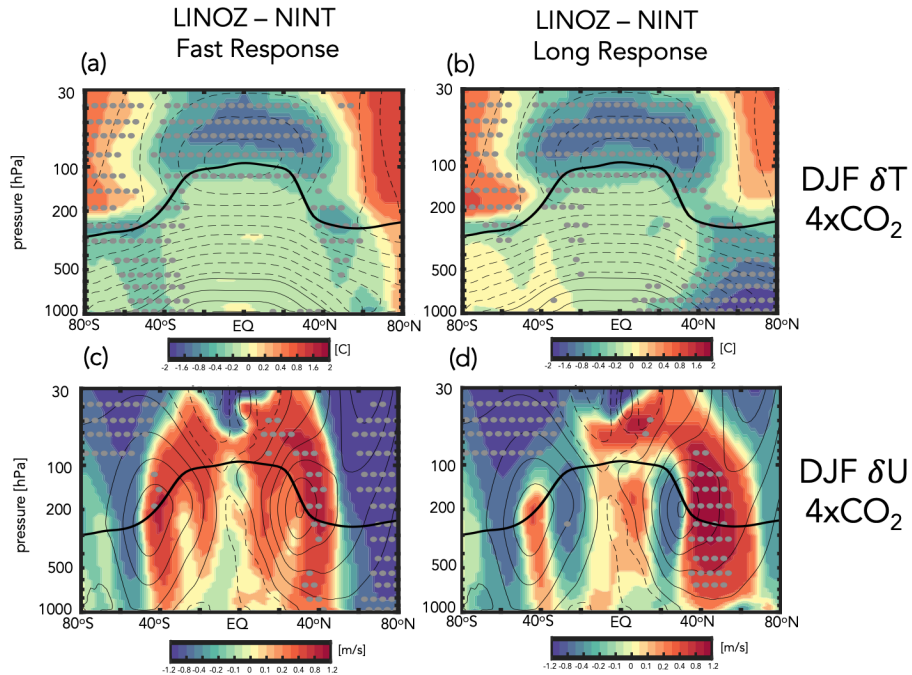
319 to reduced upwelling, adiabatic cooling, and ozone transport within the lower tropical stratosphere.  
320 These circulation changes are therefore not the primary drivers of the temperature response; rather,  
321 they are primarily determined by the shortwave radiative response to ozone changes (CP2019).

322 Despite the somewhat stronger cooling in OMA (Fig. 4c) compared to NINT (Fig. 4d), the  
323 temperature response in both configurations is within the 2-4 K range documented in CP2019 (note  
324 that all colorbars used are consistent with that study to facilitate comparisons with their results).  
325 An important point to note is that the temperature changes due to ozone are of a similar magnitude  
326 to the temperature changes due to 4xCO<sub>2</sub> alone in the tropical lower stratosphere (i.e., considering  
327 no ozone feedback), where the stratosphere cools by ~2K in the NINT ensemble (not shown). The  
328 ozone changes present in LINOZ (and OMA) therefore represent a substantial feedback on the  
329 CO<sub>2</sub>-induced cooling in the stratosphere.

### 330 *c. Ozone Feedback on Northern Hemisphere Jet: Fast Response*

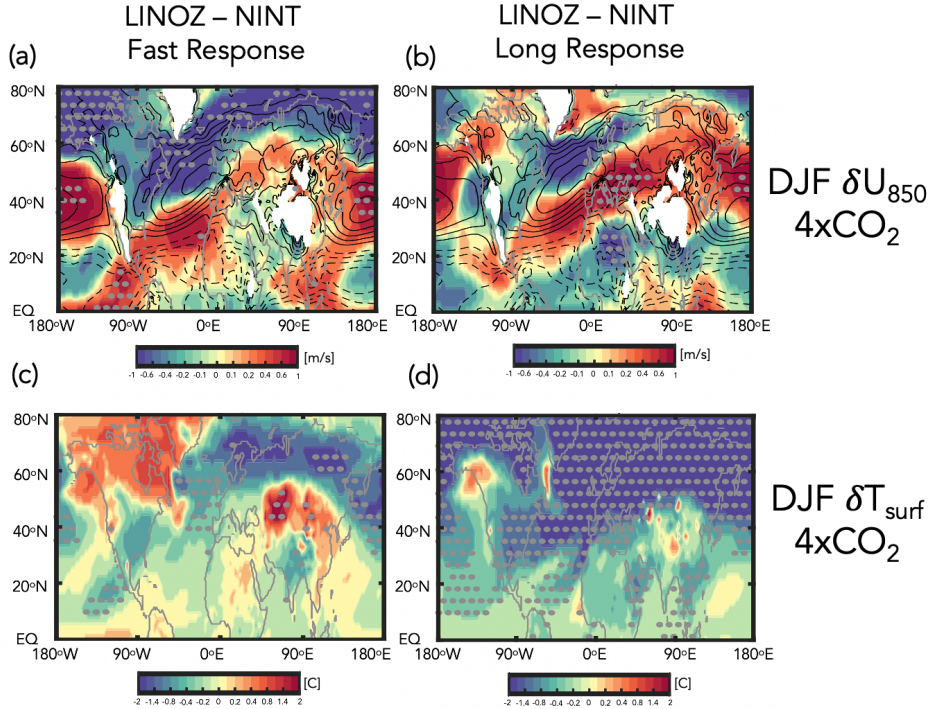
331 The temperature response due to ozone is dynamically consequential for the troposphere to the  
332 extent that it modifies temperature gradients (and winds) in the lower stratosphere. Indeed, the  
333 LINOZ ensemble shows a strong enhancement of lower stratospheric temperature gradients in both  
334 hemispheres on both the fast and long response timescales (Fig. 5a,b). In the fast response, this  
335 reduction in the meridional temperature gradient near the tropopause has important consequences  
336 for the midlatitude jet in both hemispheres, particularly in the NH where it strengthens above and  
337 along the jet core and weakens on the poleward flank of the jet over latitudes north of ~ 50°N (Fig.  
338 5c). The winds also accelerate equatorward of the jet core, relative to NINT, in both hemispheres,  
339 although the response is only statistically significant in our model in the NH. This ozone-induced  
340 response in the jet is very similar to the pattern of the wind response reported in CP2019 (see  
341 their Figures 4 and 5). As with the temperature changes occurring in the lower stratosphere, the  
342 wind response to ozone changes is similar in magnitude to the 4xCO<sub>2</sub> response, again suggesting  
343 a substantial modulation of the circulation in both hemispheres by ozone changes alone.

350 The fast zonal mean response to ozone changes reflects a weakening of the polar jet over all  
351 longitudes, with the largest negative anomalies concentrated over the Atlantic ocean which are  
352 flanked equatorward by positive wind anomalies (Fig. 6a). These wind changes are vertically  
353 coherent throughout the troposphere as the LINOZ-NINT changes are similar at 300 hPa (not



344 FIG. 5. Colors show the LINOZ-NINT ensemble mean difference in the DJF response of the zonal mean  
 345 temperatures,  $T$  (top) and zonal winds,  $U$  (bottom) in response to an abrupt quadrupling of  $\text{CO}_2$ . Both LINOZ  
 346 and NINT ensembles consist of four members. Responses are decomposed into “fast” (a,c) and “long” (b,d)  
 347 changes. Contours denote climatological mean DJF values ( $T$  contour interval: 10 C;  $U$  contour interval: 8 m/s).  
 348 Stippled regions are statistically significant and the black thick line shows the climatological mean tropopause in  
 349 the preindustrial control simulation.

354 shown). This LINOZ-NINT wind dipole over the Atlantic is very similar to the fast wind response  
 355 captured in the fully interactive OMA simulation (Fig. 3c), especially over the Atlantic. Over the  
 356 Pacific, by comparison, the OMA and LINOZ responses are different, consistent with CP2019 who  
 357 found no robust ozone feedback over the Pacific (see their Figure 5). Furthermore, the weakening  
 358 of the North Atlantic jet in the LINOZ simulations is associated with warming over North America  
 359 and cooling over the North Atlantic and over Eurasia, resembling the negative phase of the NAO  
 360 (Fig. 6c). A similar surface temperature anomaly was identified in CP2019 (see their Figure 7)  
 361 and in our model occur in conjunction with positive sea level pressure (SLP) anomalies over the  
 362 Arctic (Appendix Figure 2, top), both features being reminiscent of a negative NAO.



363 FIG. 6. Same as Figure 5, except showing the LINOZ-NINT DJF response in the 850 hPa zonal winds,  $U_{850}$   
 364 (top) and surface temperatures,  $T_{\text{surf}}$  (bottom). Contours in top panels denote climatological mean DJF values  
 365 of  $U_{850}$  (contour interval: 2 m/s). Note the similarity between the “fast” wind response shown in (a) and the  
 366 CP2019 results (their Figure 6).

367 *d. Ozone Feedback on Northern Hemisphere Jet: Long Response*

368 Interestingly, while the fast responses in the winds and temperatures in the LINOZ ensemble  
 369 are highly consistent with the results from CP2019, our model also simulates a distinct “long”  
 370 response characterized by strong cooling over the Arctic from the surface to the mid-to-upper  
 371 troposphere (Fig. 5b). This cooling, which was not identified in CP2019, results in enhanced  
 372 mid-to-lower tropospheric temperature gradients, prompting a strong poleward shift of the NH jet  
 373 and a statistically significant acceleration of the winds at 50°N exceeding 2 m/s (Fig. 5d).

374 Zonally, the cooling over the Arctic occurring in the LINOZ ensemble during the long response  
 375 primarily reflects hemispheric-wide cooling over the Arctic associated with an expansion of the  
 376 North Atlantic Warming Hole (Fig. 6d). This enhancement of meridional temperature gradients  
 377 in the lower and mid troposphere drives a poleward shift that spans all longitudes and originates  
 378 over the North Atlantic (Fig. 6b), where the jet exhibits a distinct acceleration and eastward

379 extension over Europe. Note that over the jet core (40°N-50°N) the winds accelerate (in the zonal  
380 mean) during both “fast” (Fig. 5c) and “long” responses (Fig. 5d). However, north of 50°N the  
381 responses are very different, with the fast response exhibiting a strong weakening, in contrast to  
382 the acceleration occurring on longer (i.e., “long” response) timescales. This behavior north of 50°N  
383 was not captured in CP2019 and comprises a coupled ozone-ocean feedback that is distinct from  
384 what was outlined in that study.

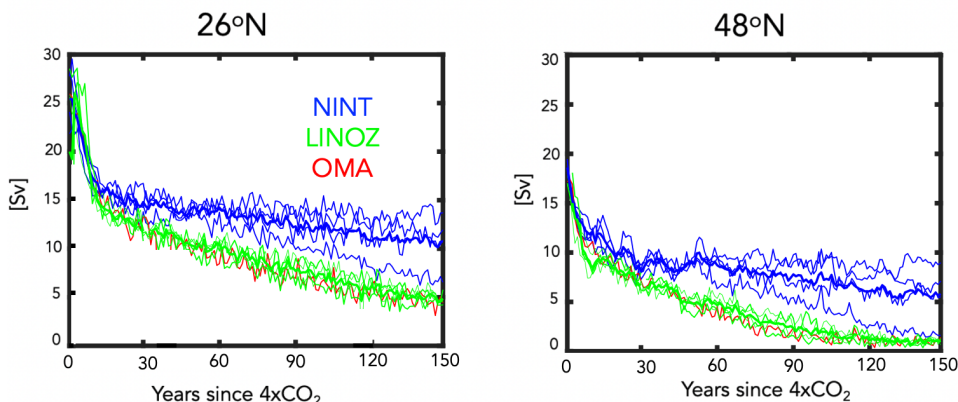
#### 385 *e. Long Ozone Feedback: Modulation by the AMOC*

386 The “long” responses in the tropospheric winds and temperatures that occurs in the LINOZ  
387 ensemble are not obviously linked to ozone-driven temperature changes in the stratosphere, which  
388 do not extend into the troposphere. What, then, is the driver of the lower tropospheric high latitude  
389 cooling, if it is not directly linked to ozone-driven stratospheric temperature changes?

390 As expected from the OMA and NINT results presented in Zhang et al. (Submitted), we find  
391 that the strong cooling that occurs over the NH in the long LINOZ response is also related to a  
392 weakening of the AMOC at 4xCO<sub>2</sub> (Mitevski et al. (2021); Rind et al. (2020); Orbe et al. (Under  
393 Review)). In particular, Figure 7 shows stronger weakening of the AMOC in the LINOZ (green  
394 lines) ensemble, relative to NINT (blue lines) at both 26°N (left) and at 48°N (right). Despite large  
395 internal variability, the LINOZ ensemble shows a more rapid decline of the AMOC, a difference  
396 that is evident at both latitudes.

401 Interestingly, comparisons of the AMOC behavior in LINOZ with the fully interactive OMA  
402 simulation (red line) shows a striking similarity (and the mechanism of these changes is also  
403 similar, as shown in Section 3f). This similarity is surprising, given that other (non-ozone) trace  
404 gases and aerosols are also evolving in the OMA experiment. In particular, Rind et al. (2018),  
405 using a previous version of the model, observed an indirect effect of natural aerosols (primarily  
406 sea salt) on AMOC stability. They showed that aerosols enhanced the local cooling of SSTs  
407 in regions of increased cloud cover in a warmer climate by acting as condensation nuclei and  
408 thereby raising cloud optical thickness and ocean surface cooling. This surface cooling was then  
409 linked to reduced evaporation relative to precipitation, resulting in anomalously positive surface  
410 freshwater forcing and reduced North Atlantic Deep Water (NADW) production. That study,  
411 however, focused on aerosol-induced AMOC cessations occurring on multicentennial timescales

## Annual Mean 4xCO<sub>2</sub> AMOC Response



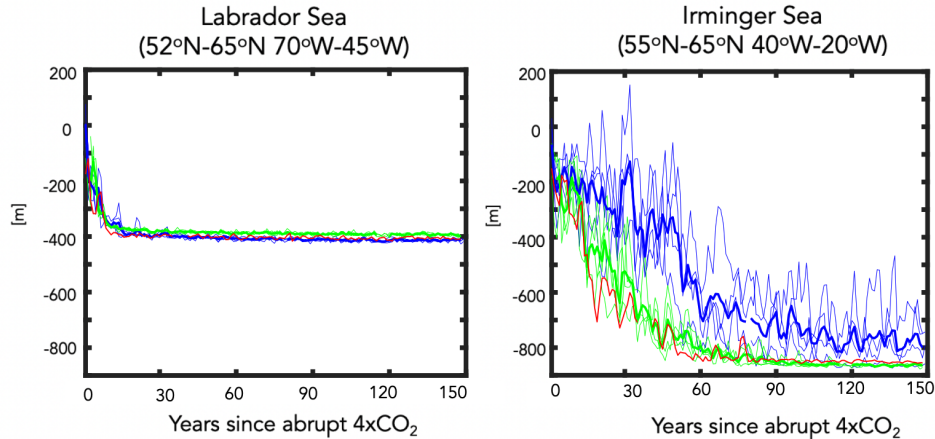
397 FIG. 7. Changes in the annual mean maximum overturning stream function in the Atlantic ocean, evaluated at  
 398 26°N (left) and 48°N (right) in response to 4xCO<sub>2</sub>, relative to the preindustrial control simulations. Results for  
 399 the LINOZ and NINT ensembles are shown in green and blue, respectively (thick lines denote ensemble means).  
 400 Red lines show the response in the OMA simulation.

412 long after the initial (abrupt) warming. By comparison, the results in Figure 7 identify an impact  
 413 of ozone on the AMOC that occurs within the first 20 years of the initial CO<sub>2</sub> forcing – that is,  
 414 over the period during which stratospheric temperature gradients are most impacted by ozone (not  
 415 aerosols). Our results, therefore, highlight that during this time frame the AMOC can be as (if not  
 416 more) sensitive to wind-driven buoyancy changes forced by stratospheric ozone anomalies as they  
 417 are to aerosol-induced changes in freshwater forcing.

418 Before elucidating the mechanism of the AMOC changes in the LINOZ ensemble, we first  
 419 identify the region over which the largest differences in mixed layer depth begin to emerge between  
 420 the LINOZ (OMA) and NINT simulations. In particular, the weaker AMOC in the LINOZ and  
 421 OMA runs is found to be accompanied by a rapid reduction in mixed layer depths, which occur  
 422 primarily in the Irminger Sea region (55°N–65°N, 40°W–20°W) (Figure 8). The mixed layer depth  
 423 differences in the Labrador Sea are, by comparison, negligible. East of the Irminger Sea (i.e.,  
 424 55°N–65°N, 20°W–0°) we also identify differences between the ensembles (not shown), but these  
 425 emerge later, suggesting that the Irminger Sea changes are likely the initiators of the differences  
 426 in AMOC behavior between the NINT and LINOZ ensembles. A similar region was identified  
 427 in Romanou et al. (Under Review) as being key for determining the sensitivity of the AMOC in



## DJF 4xCO<sub>2</sub> Response in Mixed Layer Depth



430 FIG. 8. Changes in the DJF mixed layer depths, evaluated over the Labrador Sea (left) and Irminger Sea  
431 (right) in response to 4xCO<sub>2</sub>, relative to the preindustrial control simulations. Results for the LINOZ and NINT  
432 ensembles are shown in green and blue, respectively (thick lines denote ensemble means). Red lines show the  
433 response in the OMA simulation.

428 various SSP 2-4.5 ensemble runs, albeit for simulations conducted using the low-top GISS climate  
429 model.

### 434 *f. Ozone Feedback Dependence on the AMOC: Linking Fast and Long Responses*

435 Is the fact that the AMOC declines more rapidly in the LINOZ ensemble – and the OMA run  
436 – a response to the ozone changes in those simulations or just a random occurrence? In the fast  
437 response the zonal wind changes over the North Atlantic reflect a weakening of the jet core that is  
438 flanked equatorward by positive anomalies, resembling a negative NAO pattern. Indeed, a negative  
439 (positive) NAO has been associated with a weaker (stronger) AMOC by adding (extracting) heat  
440 to/from the subpolar gyre, resulting in reduced (increased) NADW formation (Delworth and Zeng  
441 (2016)). Here we argue that such a mechanism is present in our model simulations, resulting in  
442 an additional substantial modulation of the NH midlatitude jet location by ozone, this time via its  
443 influence on the AMOC.

444 In particular, Figure 9 shows maps of the surface zonal wind, surface friction speed, mixed layer  
445 depth, net heat fluxes, sea surface temperatures, and north-south heat and salinity ocean transports



446 over years 1-5. In response to an abrupt quadrupling of CO<sub>2</sub>, there is a weak acceleration of the  
447 surface zonal winds on the poleward flank of the North Atlantic jet (~60°N-70°N) (Fig. 9a, top).  
448 Over the subpolar North Atlantic the surface winds weaken, leading to a significant reduction in  
449 surface friction speed (Fig. 9b, top) and mixed layer depths (Fig. 9c, top), as well as increased  
450 heat flux into the ocean (in the form of reduced latent heat fluxes out of the ocean) (Fig. 9d, top)  
451 and warmer sea surface temperatures (Fig. 9e, top). At these early years the changes in meridional  
452 heat and salinity transports over the Irminger Sea are relatively small (Fig. 9fg, top).

453 In response to the ozone changes captured in the LINOZ ensemble during years 1-5, there is a  
454 strong reduction in the surface zonal winds and friction speed (Fig. 9 ab, bottom), consistent with  
455 the negative NAO response evident in the 850 hPa zonal winds (Fig. 6c, top). The surface friction  
456 changes align closely with the reduced mixed layer depths which extend well into the Irminger Sea  
457 region and over latitudes further south of the subpolar gyre (Fig. 9c, bottom).

458 The reductions in mixed layer depth that occur over the Irminger Sea are likely driven by the  
459 reductions in surface wind speed which increased (primarily latent) heat fluxes into the ocean  
460 (Fig. 9d, bottom), driving warmer sea surface temperatures in LINOZ, relative to NINT (Fig. 9e,  
461 bottom). The sign of the response of the heat fluxes in the subpolar gyre region is consistent with  
462 previous studies showing that a positive (negative) phase of the NAO implies reduced (enhanced)  
463 atmosphere to ocean heat fluxes (Delworth et al. (2017)). Furthermore, the spatial pattern of  
464 the heat flux response is very similar to the NAO heat flux composites that were prescribed in  
465 Delworth and Zeng (2016) and inferred from observations in Ma et al. (2020) (see their Figure  
466 6), who showed that there is much greater heat loss from the ocean over the subpolar region in  
467 association with a jet strengthening.

468 At the same time, the changes in freshwater forcing (P-E) during this time period are negligible  
469 such that the net buoyancy forcing (~Q+F) is positive. This stabilizing buoyancy forcing from sur-  
470 face warming makes the mixed layer depths shallower by suppressing convective mixing, shutting  
471 down NADW production (Alexander et al. (2000); Kantha and Clayson (2000)). There is also an  
472 initial change in the north-south heat and salt transports that is collocated with the dipole anomaly in  
473 the surface friction speed, promoting anomalous poleward salt and heat transport into the subpolar  
474 gyre (Fig. 9fg, bottom). This feature is confined to the top few ocean layers (not shown) and the

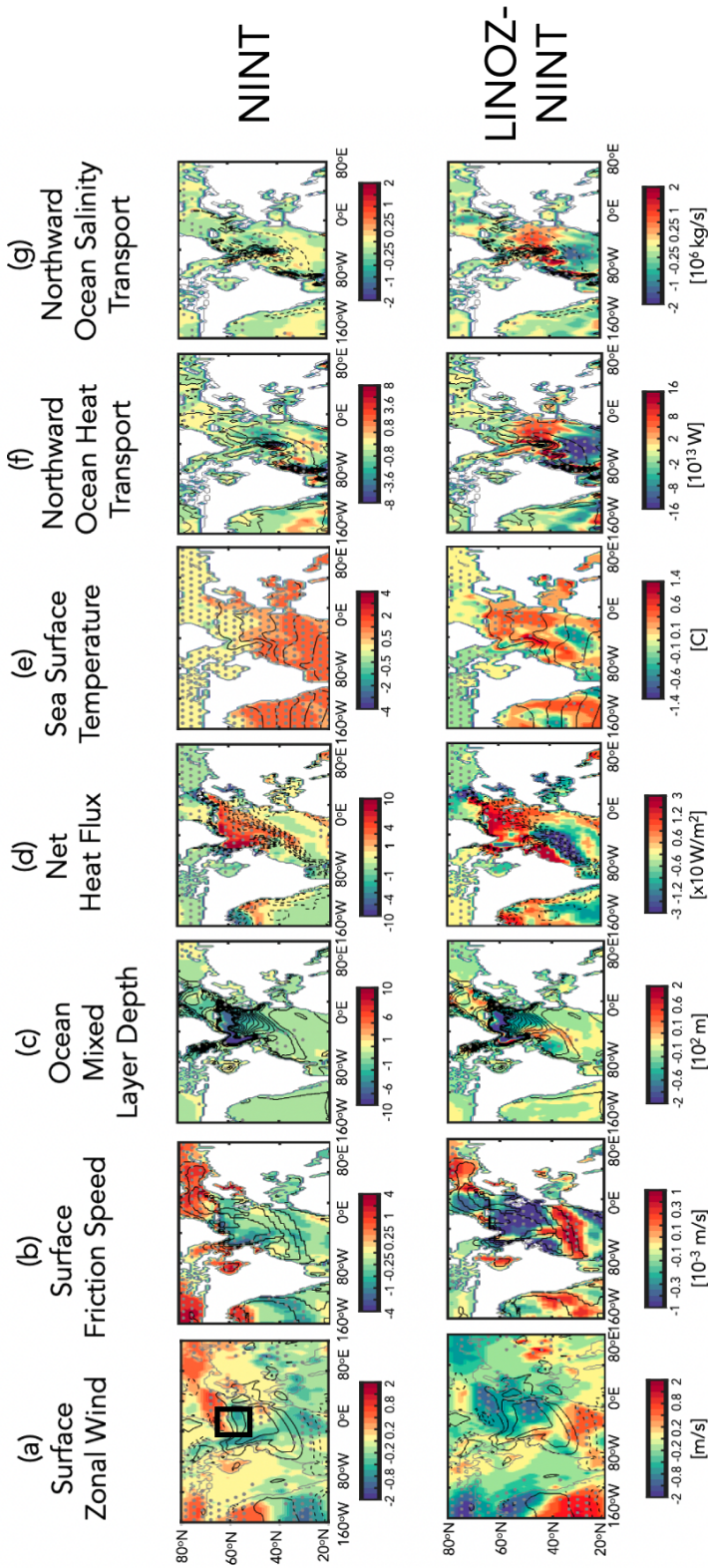
475 implied anomalous heat transport could be contributing to the warmer sea surface temperatures in  
476 that region, in addition to the surface heat flux changes.

485 Over the ensuing years (5-20) a similar pattern is maintained in the LINOZ ensemble (Figure  
486 10, middle row). The reduction in NADW, however, results in reduced northward heat and salinity  
487 transports (Fig. 10 fg, middle) throughout the ocean column. While this results in cooler SSTs  
488 south of the subpolar gyre region (Fig. 10e, middle), which otherwise might enhance the density  
489 of the near-surface water masses, the reduced northward salinity transports prevent the AMOC  
490 from restarting. Interestingly, the results from the OMA simulation show a very similar response  
491 as the LINOZ ensemble (Figure 10, bottom row), suggesting that stratospheric ozone changes in  
492 that simulation are also likely the primary driver of the weaker AMOC in that model configuration.  
493 This sequence of processes linking the surface wind changes to anomalous heat fluxes and reduced  
494 NADW is basically identical to what is outlined in Figure 4 of Delworth and Zeng (2016) and  
495 Figure 1 of Khatri et al. (2022). Additional analysis of the 2xCO<sub>2</sub> simulations, which feature a  
496 stronger AMOC decline in OMA (and LINOZ) compared to NINT (Figure 2), reveals that a similar  
497 mechanism for reduced NADW production occurs at lower CO<sub>2</sub> forcing (not shown).

501 Finally, examining the timescale of the responses of the variables shown in Figures 9 and  
502 10 reinforces the strong coupling between the changes in surface friction speed, sea surface  
503 temperature, latent heat fluxes and mixed layer depth changes over the Irminger Sea region (Figure  
504 11a-d). Despite large internal variability, there is a clear separation between the LINOZ (and  
505 OMA) and NINT ensembles that emerges around year 15 (black dashed lines). The changes in  
506 sensible heat emerge after the latent heat fluxes (Fig. 11e), suggesting that the latter play a more  
507 important contribution in initializing the heat flux differences in LINOZ (and OMA), relative to  
508 NINT.

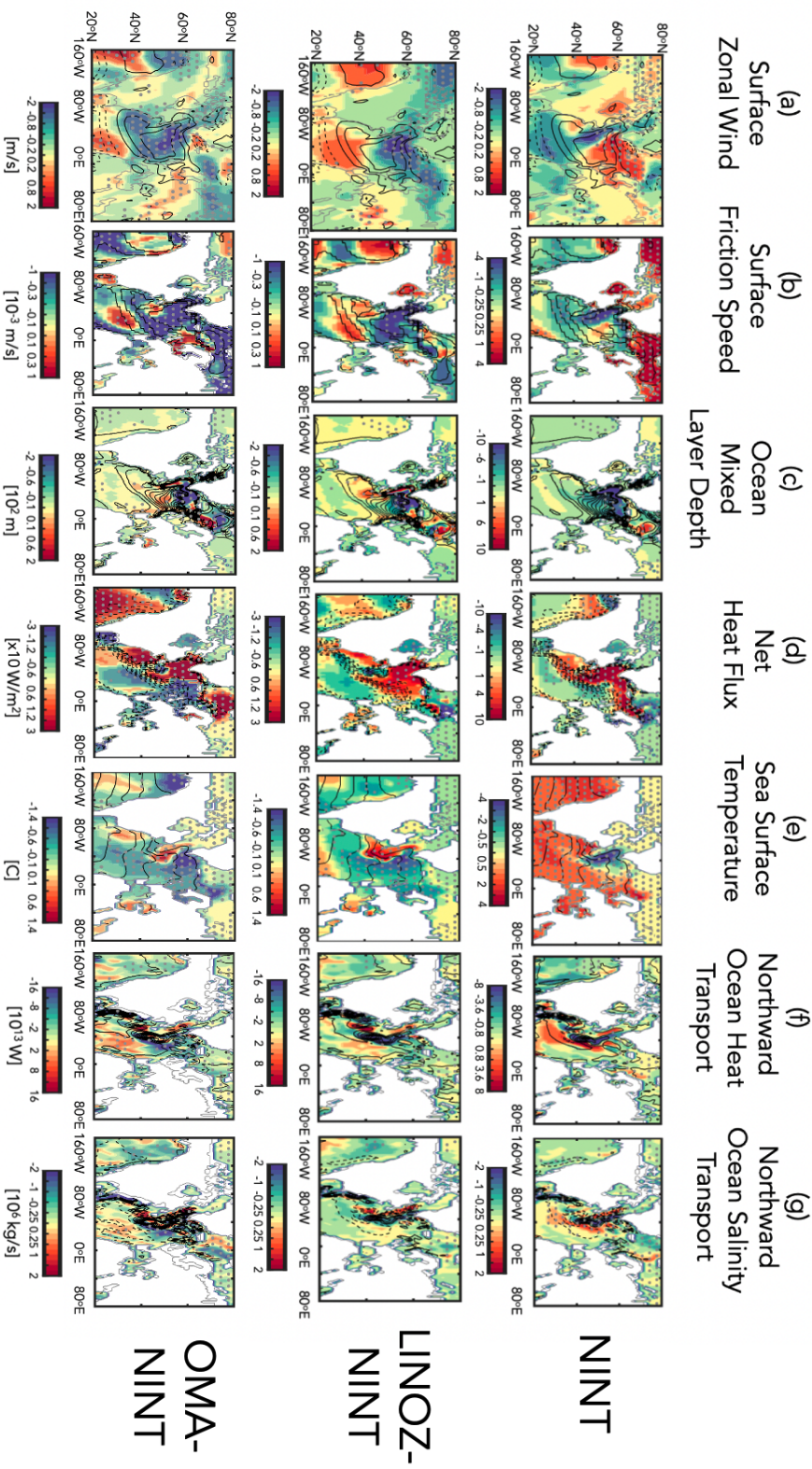
509 Finally, while they may contribute to enhanced positive buoyancy forcing later in the integrations,  
510 the freshwater forcing anomalies ( $F = P - E$ ) are shown to be negligible during the initial years  
511 following the abrupt quadrupling of CO<sub>2</sub> (Fig. 11f), indicating that the primary driver of the  
512 initial difference between the LINOZ (and OMA) and NINT runs is related to the surface wind-  
513 driven changes as they impact the latent heat fluxes into the ocean. This is consistent with Roach  
514 et al. (2022) who showed a much stronger correlation between AMOC strength at 26°N and the  
515 heat component of the surface buoyancy flux, relative to the freshwater component, in various

# DJF 4xCO<sub>2</sub> Response over Years 1-5



477 Fig. 9. Top panels: Colors show the December-January-February (DJF) response of the surface zonal wind (a), surface friction speed (b), ocean mixed  
 478 layer depth (c), net heat flux (sum of sensible plus latent heat) (d), sea surface temperature (e) and northward heat (f) and salt (g) transports in response  
 479 to an abrupt quadrupling of CO<sub>2</sub>. Results are shown for the 4-member ensemble averaged NINT configuration. Bottom panels: Same as top panels,  
 480 except showing the LINOZ minus NINT ensemble mean difference. For both top and bottom panels, responses have been averaged over years 1-5 since  
 481 “branching” from the preindustrial control simulation. Stippled regions are statistically significant and black contours denote climatological mean DJF  
 482 values. Contour intervals: surface zonal wind [2 m/s], surface friction speed [ $2.5 \times 10^{-3}$  m/s], mixed layer depth [60 m], net heat flux [ $30 \text{ W/m}^2$ ], sea  
 483 surface temperature interval [2 C], northward heat flux [ $2 \times 10^{12}$  W], and northward salt flux [ $10^6$  kg/s]. The black box in (a) bounds the Irminger Sea  
 484 region over which the spatial averages in Figure 8b and Figure 11 are evaluated.

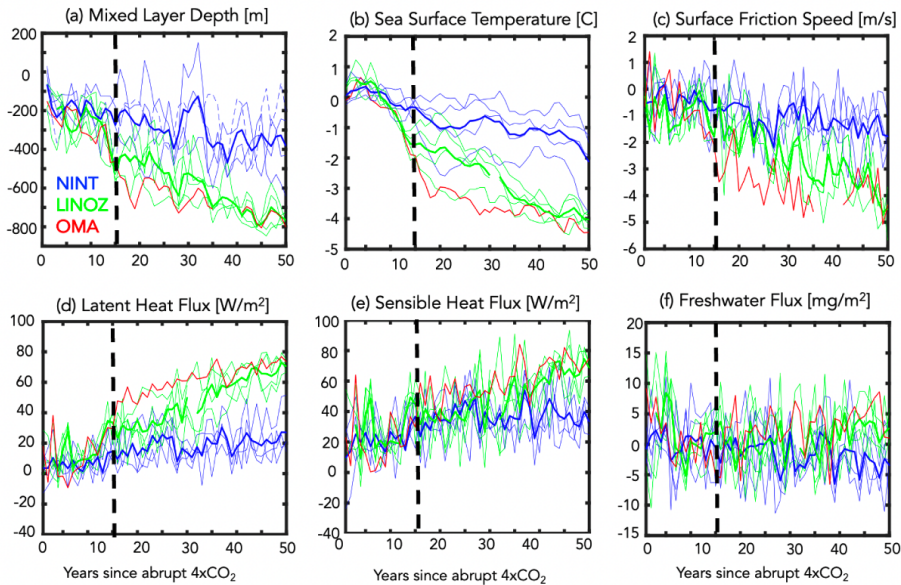
# DJF 4xCO<sub>2</sub> Response over Years 5-20



498 FIG. 10. Same as Figure 9, except showing the responses, averaged over years 5-20. An extra row at the bottom has been added, showing the OMA -  
 499 NINT differences, where the ensemble members shown in Figures 1, 2 and 3 have been used. Same contour intervals and colorbars have been used as  
 500 in Fig. 9.



## DJF 4xCO<sub>2</sub> Response over Irminger Sea



521 FIG. 11. Changes in the DJF mixed layer depths (a), sea surface temperatures (b), surface friction speed (c),  
 522 latent heat fluxes (d), sensible heat fluxes (e) and precipitation minus evaporation (f) in response to 4xCO<sub>2</sub>,  
 523 relative to the preindustrial control simulations. Averages are over the Irminger Sea (55°N-65°N, 40°W-20°W).  
 524 Results for the LINOZ and NINT ensembles are shown in green and blue, respectively (thick lines denote  
 525 ensemble means). Red lines show the response in the OMA simulation. Black vertical lines indicate year  
 526 ~15 at which point the mixed layer depth responses in the LINOZ and NINT ensembles diverge. Note that  
 527 the freshwater flux unit of 1 mg/m<sup>2</sup> per second ( $\equiv 0.0864$  mm/day  $\equiv 3.1$  cm/year) is used, because at 5°C it  
 528 contributes approximately the same ocean density flux as the heat flux unit of 1 W/m<sup>2</sup> (Large and Yeager (2009)).

516 experiments using the Community Earth System Model version 1 (CESM1) in which the winds  
 517 over the subpolar gyre were nudged to reanalysis values. Note that in our model other potential  
 518 contributors to freshwater forcing from sea ice do reveal differences between the LINOZ, OMA  
 519 and NINT ensembles, but these emerge several years (i.e., years ~20-30) after the changes in sea  
 520 surface temperatures and heat fluxes (not shown).

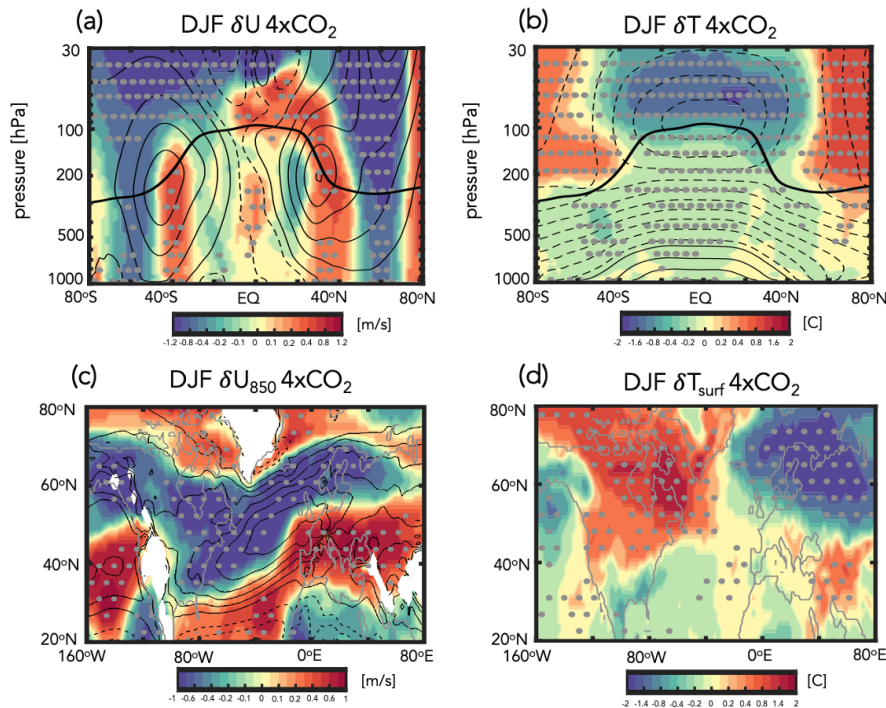
529 *g. Ozone Driver of AMOC Changes: Fixed SST Results*

530 So far, we have shown that the stratospheric ozone changes that occur in response to 4xCO<sub>2</sub>  
531 result in a negative NAO response over the North Atlantic (Fig. 5,6). In our model this triggers a  
532 more rapid decline of the AMOC (Fig. 7) through surface-wind driven changes in heat fluxes into  
533 the ocean (Fig. 9,10). While the time series analysis (Fig. 11) reveals that the AMOC changes  
534 in the LINOZ (OMA) ensemble occur on similar timescales as the wind (and heat flux) changes,  
535 one potentially confounding factor is the fact that the AMOC reduction itself results in reduced  
536 wind speeds over the subpolar gyre region. These reduced near-surface winds are associated with  
537 an anomalous anticyclonic flow pattern (Appendix Figure 2, top) (Gervais et al. (2019); Romanou  
538 et al. (Under Review); Orbe et al. (Under Review)), which could contribute to the reduced heat  
539 fluxes and subsequent changes in NADW production. Therefore, to more convincingly link the  
540 surface wind speed changes to the stratospheric ozone changes aloft, we next examine results from  
541 the fixed SST experiments.

542 Figure 12 shows the ozone-induced zonal wind and temperature changes averaged over the last  
543 twenty years of the fixed SST and SIC experiments in which the ensemble mean ozone 4xCO<sub>2</sub>  
544 evolution from LINOZ is prescribed (Fig. 12 a,b). Recall that in the fixed SST experiment, only  
545 the ozone evolution differs from the preindustrial control simulation, as CO<sub>2</sub>, SSTs and SIC are  
546 all set to preindustrial values. Comparisons with results from the fully coupled LINOZ “fast”  
547 response (see Fig. 5a,c) reveal a very similar picture. This similarity between the fully coupled fast  
548 response and the fixed SST and SIC experiment is striking, both featuring a similar change in the  
549 NH jet associated with enhanced temperature gradients in the lower stratosphere as first reported  
550 in CP2019.

551 Comparisons of the 850 hPa zonal winds and surface temperatures over the North Atlantic (Fig.  
552 12c,d) also reveal a strikingly similar response between the fully coupled ensemble and the fixed  
553 SST experiments (compare with Fig. 6a,c). Note this similar response extends to sea level pressure  
554 as well (Appendix Figure 2, bottom). This result is interesting as it suggests that over the North  
555 Atlantic stratospheric ozone changes alone can result in a significant reduction in the near surface  
556 winds that is on the same order (if not larger than) the 4xCO<sub>2</sub> response. In our coupled atmosphere-  
557 ocean model this additionally results in heat flux changes that are large enough to reduce NADW  
558 production, resulting in a significant (i.e. 30-40%) change in AMOC strength.

## LINOZ – NINT Fixed SST Changes



559 FIG. 12. Top panels: Colors show the 4xCO<sub>2</sub> ensemble mean response in zonal mean zonal winds, U (a),  
 560 temperatures, T (b), 850 hPa zonal winds, U<sub>850</sub> (c) and surface temperature, T<sub>surf</sub> (d) in the AMIP experiments in  
 561 which the time-evolving 4xCO<sub>2</sub> ensemble mean LINOZ ozone response is prescribed. Note that SSTs, SICs and  
 562 background CO<sub>2</sub> are all set to preindustrial values. Averages are shown over the last 20 years (years 40-60) of the  
 563 integrations. Black contours, where shown, denote climatological mean DJF values (U contour interval: 8 m/s;  
 564 T contour interval: 10 C; U<sub>850</sub> contour interval: 2 m/s). Stippled regions are statistically significant and the black  
 565 thick line in the top panels shows the climatological mean tropopause in the preindustrial control simulation.

## 566 4. Conclusions

567 Here we have used the NASA GISS coupled atmosphere-ocean high-top model (E2.2-G) to  
 568 examine how coupled changes in stratospheric ozone and the ocean circulation both influence the  
 569 4xCO<sub>2</sub> response of the NH midlatitude jet. Our key results are as follows:

- 570 • The NH midlatitude jet response to 4xCO<sub>2</sub> is modulated by coupled feedbacks from both  
 571 stratospheric ozone and the AMOC, which occur of “fast” (5-20 year) and “long” (100-150  
 572 year) timescales, respectively.

- 573 • In the “fast” response, the zonal mean jet weakens (strengthens) on its poleward (equatorward)  
574 flank, consistent with reduced LS temperature gradients associated with ozone loss in the  
575 tropics. Zonally, this jet change is expressed as a negative NAO-like pattern, consisting of  
576 weaker zonal surface winds over the North Atlantic, consistent with the findings in CP2019.
- 577 • The weaker winds over the North Atlantic are associated with increased (primarily latent) heat  
578 fluxes into the ocean, which initially result in warmer SSTs over the subpolar gyre region,  
579 reducing NADW production and leading to more rapid weakening of the AMOC.
- 580 • A reduced AMOC leads to widespread cooling over the Arctic which enhance mid-to-lower  
581 tropospheric temperature gradients, resulting in a poleward shift of the NH midlatitude jet.  
582 This “long” response is consistent with previous studies showing that a weakening of the  
583 AMOC results in a stronger and poleward shifted jet in the NH (e.g., Bellomo et al. (2021);  
584 Orbe et al. (Under Review); Liu et al. (2020); Zhang et al. (Submitted)).

585 Taken together, the findings listed above indicate that the stratospheric ozone feedback on the NH  
586 midlatitude jet reported in CP2019 is coupled to the behavior of the AMOC during the “fast”  
587 response, wherein the jet weakens over the North Atlantic. In our model, this wind response  
588 extends to the surface, resulting in reduced heat fluxes out of the subpolar gyre region and a more  
589 rapid decline of the AMOC. On longer timescales, these changes in the AMOC subsequently  
590 drive a poleward shift in the NH midlatitude jet. Unlike the “fast” response, this “long” timescale  
591 response in the NH jet to changes in stratospheric ozone has not been previously reported, to the  
592 best of our knowledge. This may reflect the fact that many of the stratosphere resolving chemistry  
593 climate models that are used to inform future projections of stratospheric ozone (Eyring et al.  
594 (2008); Fahey et al. (2018)), are not always run coupled to an interactive ocean (Morgenstern et al.  
595 (2017)). Among those that are run coupled to a dynamic ocean, our results will, of course, need to  
596 be tested to assess robustness.

597 Another intriguing result from this study is that the stronger decline of the AMOC in the LINOZ  
598 ensemble does not appear to be a random occurrence. Rather, in our model, the “fast” ozone  
599 and “long” AMOC feedbacks on the NH jet are coupled through surface-wind driven changes in  
600 heat fluxes into the ocean. Key here is the fact that this sensitivity in the AMOC is driven only  
601 by changes in stratospheric ozone, which we have isolated from changes in other trace gases and



602 aerosols. Thus, while previous studies (Rind et al. (2018)) have identified an important influence of  
603 interactive composition on the AMOC, they have mainly implicated the indirect effect of aerosols  
604 on clouds through changes in sea surface temperatures and how these impact P-E (and net surface  
605 freshwater forcing). To the best of our knowledge, no study has previously demonstrated an impact  
606 of stratospheric ozone changes alone on the AMOC response to a quadrupling of CO<sub>2</sub>. Despite the  
607 different mechanisms at play, however, are results are generally consistent with those from Rind  
608 et al. (2018) in highlighting the need for renewed focus on surface flux observations to help assess  
609 overturning stability.

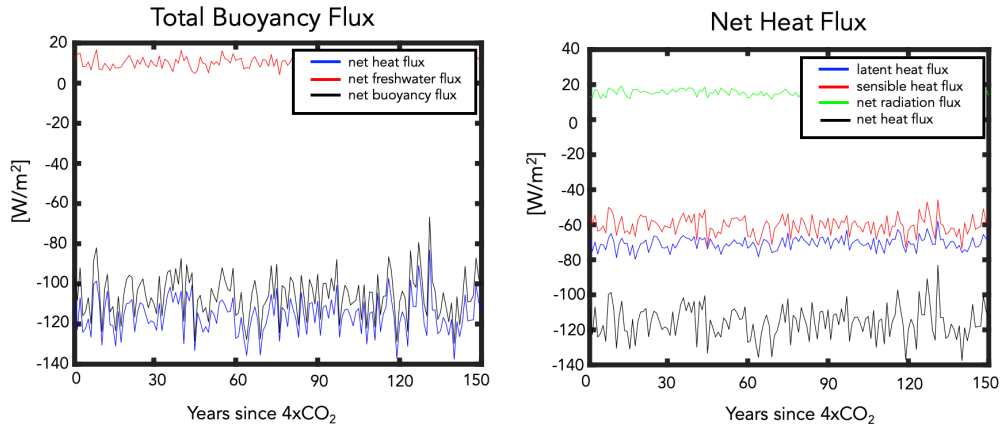
610 An important caveat with our results is related to known biases in vertical mixing and NADW  
611 production in the ocean component of the GISS model (Miller et al. (2021); Romanou et al. (Under  
612 Review)) which likely explain why the low-top version of the coupled atmosphere-ocean climate  
613 model (E2.1-G) exhibits a more sensitive AMOC response to a quadrupling of CO<sub>2</sub>, compared to  
614 some other models (Bellomo et al. (2021)). At the same time, the high-top model employed in this  
615 study is much less sensitive, as the AMOC weakens by ~10 SV in response to 4xCO<sub>2</sub>, compared  
616 to a complete collapse in E2.1-G (see Figure 31 in Rind et al. (2020)). That study showed that this  
617 may be related to differences in the parameterization of rainfall evaporation associated with moist  
618 convective precipitation, which they show has a strong influence on the AMOC sensitivity in the  
619 GISS model via its effect on moisture loading in the atmosphere. While an exhaustive comparison  
620 between the models is beyond the scope of this study, the relevant point here is that the 4xCO<sub>2</sub>  
621 AMOC response simulated in the E2.2-G NINT ensemble is well within the CMIP5 and CMIP6  
622 ranges documented in Mitevski et al. (2021) (see their Supplementary Figure S3).

623 Finally, our results linking the fast timescale jet response to the ensuing AMOC changes un-  
624 derscore the profound impact that changes in lower stratospheric winds alone can have on surface  
625 climate, as highlighted in Sigmond and Scinocca (2010). Quite remarkably, our fixed SST and SIC  
626 experiment showed that these lower stratospheric wind changes are driven primarily by changes  
627 in ozone and not by background changes in CO<sub>2</sub> or in sea surface boundary conditions. Taken  
628 together, our results suggest that more attention needs to be paid to understanding the time-evolving  
629 response of the coupled Earth system to future ozone changes, with a focus on changes in ocean  
630 heat transport and how these feed back on the NH jet stream.

631 *Acknowledgments.* C.O. acknowledges useful discussions with Lorenzo Polvani and Ivan  
632 Mitevski. Climate modeling at GISS is supported by the NASA Modeling, Analysis and Prediction  
633 program, and resources supporting this work were provided by the NASA High-End Computing  
634 (HEC) Program through the NASA Center for Climate Simulation (NCCS) at Goddard Space  
635 Flight Center.

636 *Data availability statement.* The OMA and NINT GISS E2.2-G data used in the study are  
637 available at the CMIP6 archive via the Earth System Grid Federation ([https://esgf-node.  
638 llnl.gov/](https://esgf-node.llnl.gov/)). The specific simulations used here are the piControl, abrupt-2xCO2, and abrupt-  
639 4xCO2 r1i1p1f1 (NINT) and r1i1p3f1 (OMA) runs. Output from the additional three NINT 4xCO2  
640 simulations as well the four-member LINOZ ensemble is available at [https://gmao.gsfc.  
641 nasa.gov/gmaoftp/corbe/AMOC\\_Linoz/](https://gmao.gsfc.nasa.gov/gmaoftp/corbe/AMOC_Linoz/). All GISS ModelE components are open source and  
642 available at <http://www.giss.nasa.gov/tools/modelE/>.

Annual Mean PiControl Climatological  
Flux Decompositions over the Irminger Sea



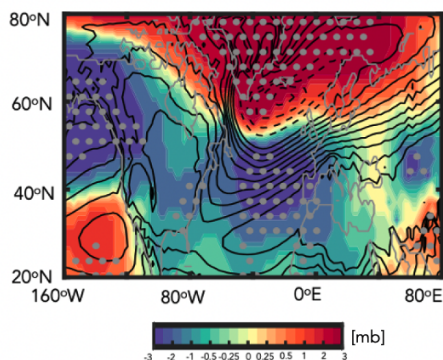
645 FIG. A1. Left: Decomposition of the net surface buoyancy flux (black) into its contributions from net heat  
646 (blue) and net freshwater (red) fluxes. Right: Further decomposition of the net surface heat flux (black) into  
647 contributions from latent heat fluxes ( $Q_E$  (blue)), sensible heat fluxes ( $Q_H$  (red)), and combined solar and  
648 longwave radiative fluxes ( $Q_S+Q_L$  (green)). Results are shown for 150 years of the NINT preindustrial control  
649 (PiControl) simulation, evaluated over the Irminger Sea.

643

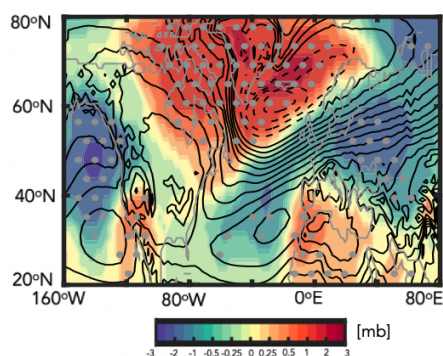
APPENDIX

644 **A1. Appendix Figures**

## DJF $\delta$ SLP 4xCO<sub>2</sub>



LINOZ – NINT  
Coupled SST



LINOZ – NINT  
Fixed SST

650 FIG. A2. Top panel: Colors show the LINOZ minus NINT ensemble mean difference in the December-January-  
651 February (DJF) “fast” response of the sea level pressure to an abrupt quadrupling of CO<sub>2</sub>. Results are shown  
652 for the fully coupled atmosphere-ocean simulations. Bottom panel: The ensemble mean response in sea level  
653 pressure in the AMIP experiments in which the time-evolving 4xCO<sub>2</sub> ensemble mean LINOZ ozone response  
654 is prescribed. Note that SSTs, SICs and background CO<sub>2</sub> are set to preindustrial values. Black contours denote  
655 climatological mean DJF values (contour interval: 10 mb). Stippled regions are statistically significant.

## 656 References

657 Alexander, M. A., J. D. Scott, and C. Deser, 2000: Processes that influence sea surface temperature  
658 and ocean mixed layer depth variability in a coupled model. *Journal of Geophysical Research:*  
659 *Oceans*, **105** (C7), 16 823–16 842.

660 Ayarzagüena, B., and Coauthors, 2020: Uncertainty in the response of sudden stratospheric  
661 warmings and stratosphere-troposphere coupling to quadrupled CO<sub>2</sub> concentrations in CMIP6  
662 models. *Journal of Geophysical Research: Atmospheres*, **125** (6), e2019JD032 345.

663 Bauer, S. E., and Coauthors, 2020: Historical (1850–2014) aerosol evolution and role on climate  
664 forcing using the GISS ModelE2. 1 contribution to CMIP6. *Journal of Advances in Modeling*  
665 *Earth Systems*, **12** (8), e2019MS001 978.

666 Bellomo, K., M. Angeloni, S. Corti, and J. von Hardenberg, 2021: Future climate change shaped  
667 by inter-model differences in Atlantic meridional overturning circulation response. *Nature Com-*  
668 *munications*, **12** (1), 1–10.

669 Booth, B. B., N. J. Dunstone, P. R. Halloran, T. Andrews, and N. Bellouin, 2012: Aerosols  
670 implicated as a prime driver of twentieth-century North Atlantic climate variability. *Nature*,  
671 **484** (7393), 228–232.

672 Butler, A. H., D. W. Thompson, and R. Heikes, 2010: The steady-state atmospheric circulation  
673 response to climate change–like thermal forcings in a simple general circulation model. *Journal*  
674 *of Climate*, **23** (13), 3474–3496.

675 Ceppi, P., and D. L. Hartmann, 2015: Connections between clouds, radiation, and midlatitude  
676 dynamics: A review. *Current Climate Change Reports*, **1** (2), 94–102.

677 Ceppi, P., G. Zappa, T. G. Shepherd, and J. M. Gregory, 2018: Fast and slow components of  
678 the extratropical atmospheric circulation response to CO<sub>2</sub> forcing. *Journal of Climate*, **31** (3),  
679 1091–1105.

680 Chiodo, G., L. M. Polvani, D. R. Marsh, A. Stenke, W. Ball, E. Rozanov, S. Muthers, and  
681 K. Tsigaridis, 2018: The response of the ozone layer to quadrupled CO<sub>2</sub> concentrations. *Journal*  
682 *of Climate*, **31** (10), 3893–3907.

683 Cowan, T., and W. Cai, 2013: The response of the large-scale ocean circulation to 20<sup>th</sup> century  
684 Asian and non-Asian aerosols. *Geophysical Research Letters*, **40** (11), 2761–2767.

685 DallaSanta, K., C. Orbe, D. Rind, L. Nazarenko, and J. Jonas, 2021a: Dynamical and trace gas  
686 responses of the Quasi-Biennial Oscillation to increased CO<sub>2</sub>. *Journal of Geophysical Research:*  
687 *Atmospheres*, **126** (6), e2020JD034 151.

688 DallaSanta, K., C. Orbe, D. Rind, L. Nazarenko, and J. Jonas, 2021b: Response of the Quasi-  
689 Biennial Oscillation to historical volcanic eruptions. *Geophysical Research Letters*, **48** (20),  
690 e2021GL095 412.

- 691 Delworth, T. L., and K. W. Dixon, 2000: Implications of the recent trend in the Arctic/North  
692 Atlantic oscillation for the North Atlantic thermohaline circulation. *Journal of Climate*, **13** (21),  
693 3721–3727.
- 694 Delworth, T. L., and F. Zeng, 2016: The impact of the North Atlantic oscillation on climate  
695 through its influence on the Atlantic meridional overturning circulation. *Journal of Climate*,  
696 **29** (3), 941–962.
- 697 Delworth, T. L., F. Zeng, L. Zhang, R. Zhang, G. A. Vecchi, and X. Yang, 2017: The central role  
698 of ocean dynamics in connecting the North Atlantic oscillation to the extratropical component  
699 of the Atlantic multidecadal oscillation. *Journal of Climate*, **30** (10), 3789–3805.
- 700 Eyring, V., S. Bony, G. A. Meehl, C. A. Senior, B. Stevens, R. J. Stouffer, and K. E. Taylor, 2016:  
701 Overview of the Coupled Model Intercomparison Project Phase 6 (CMIP6) experimental design  
702 and organization. *Geoscientific Model Development*, **9** (5), 1937–1958.
- 703 Eyring, V., and Coauthors, 2008: Overview of the new CCMVal reference and sensitivity simula-  
704 tions in support of upcoming ozone and climate assessments and the planned SPARC CCMVal  
705 report. *SPARC newsletter*, **30**, 20–26.
- 706 Fahey, D., and Coauthors, 2018: Scientific assessment of ozone depletion: 2018, Global ozone  
707 research and monitoring project-report no. 58. World Meteorological Organization.
- 708 Garcia, R. R., and W. J. Randel, 2008: Acceleration of the brewer–dobson circulation due to  
709 increases in greenhouse gases. *Journal of the Atmospheric Sciences*, **65** (8), 2731–2739.
- 710 Gervais, M., J. Shaman, and Y. Kushnir, 2019: Impacts of the North Atlantic warming hole in  
711 future climate projections: Mean atmospheric circulation and the North Atlantic jet. *Journal of*  
712 *Climate*, **32** (10), 2673–2689.
- 713 Grise, K. M., and L. M. Polvani, 2014: The response of midlatitude jets to increased CO<sub>2</sub>:  
714 Distinguishing the roles of sea surface temperature and direct radiative forcing. *Geophysical*  
715 *Research Letters*, **41** (19), 6863–6871.
- 716 Isaksen, I. S., and Coauthors, 2009: Atmospheric composition change: Climate–chemistry inter-  
717 actions. *Atmospheric Environment*, **43** (33), 5138–5192.

718 Kantha, L. H., and C. A. Clayson, 2000: *Small scale processes in geophysical fluid flows*. Elsevier.

719 Khatri, H., R. G. Williams, T. Woollings, and D. M. Smith, 2022: Fast and slow subpolar ocean  
720 responses to the North Atlantic oscillation: Thermal and dynamical changes. *Geophysical*  
721 *Research Letters*, **49 (24)**, e2022GL101480.

722 Lindzen, R. S., 1987: On the development of the theory of the QBO. *Bulletin of the American*  
723 *Meteorological Society*, 329–337.

724 Liu, W., A. V. Fedorov, S.-P. Xie, and S. Hu, 2020: Climate impacts of a weakened Atlantic  
725 meridional overturning circulation in a warming climate. *Science Advances*, **6 (26)**, eaaz4876.

726 Ma, L., T. Woollings, R. G. Williams, D. Smith, and N. Dunstone, 2020: How does the winter  
727 jet stream affect surface temperature, heat flux, and sea ice in the North Atlantic? *Journal of*  
728 *Climate*, **33 (9)**, 3711–3730.

729 Marshall, J., H. Johnson, and J. Goodman, 2001: A study of the interaction of the North Atlantic  
730 oscillation with ocean circulation. *Journal of Climate*, **14 (7)**, 1399–1421.

731 McLinden, C., S. Olsen, B. Hannegan, O. Wild, M. Prather, and J. Sundet, 2000: Stratospheric  
732 ozone in 3-D models: A simple chemistry and the cross-tropopause flux. *Journal of Geophysical*  
733 *Research: Atmospheres*, **105 (D11)**, 14653–14665.

734 Miller, R. L., and Coauthors, 2021: Cmp6 historical simulations (1850–2014) with GISS-E2. 1.  
735 *Journal of Advances in Modeling Earth Systems*, **13 (1)**, e2019MS002034.

736 Mitevski, I., C. Orbe, R. Chemke, L. Nazarenko, and L. M. Polvani, 2021: Non-monotonic  
737 response of the climate system to abrupt CO<sub>2</sub> forcing. *Geophysical Research Letters*, **48 (6)**,  
738 e2020GL090861.

739 Morgenstern, O., and Coauthors, 2017: Review of the global models used within Phase 1 of  
740 the Chemistry–Climate Model Initiative (CCMI). *Geoscientific Model Development*, **10 (2)**,  
741 639–671.

742 Nowack, P. J., N. Luke Abraham, A. C. Maycock, P. Braesicke, J. M. Gregory, M. M. Joshi,  
743 A. Osprey, and J. A. Pyle, 2015: A large ozone-circulation feedback and its implications for  
744 global warming assessments. *Nature Climate Change*, **5 (1)**, 41–45.

745 O’Callaghan, M. J. D. S., Amee, and D. Mitchell, 2014: The effects of different sudden stratospheric  
746 warming types on the ocean. *Geophysical Research Letters*, **41** (21), 7739–7745.

747 Orbe, C., and Coauthors, 2020: GISS Model E2.2: A climate model optimized for the middle  
748 atmosphere—2. Validation of large-scale transport and evaluation of climate response. *Journal*  
749 *of Geophysical Research: Atmospheres*, **125** (24), e2020JD033 151.

750 Orbe, C., and Coauthors, Under Review: Atmospheric response to a collapse of the North Atlantic  
751 circulation under a mid-range future climate scenario: A regime shift in Northern Hemisphere  
752 dynamics. *Journal of Climate*.

753 Reichler, T., J. Kim, E. Manzini, and J. Kröger, 2012: A stratospheric connection to Atlantic  
754 climate variability. *Nature Geoscience*, **5** (11), 783–787.

755 Rind, D., J. Jonas, N. Balachandran, G. A. Schmidt, and J. Lean, 2014: The QBO in two GISS global  
756 climate models: 1. Generation of the QBO. *Journal of Geophysical Research: Atmospheres*,  
757 **119** (14), 8798–8824.

758 Rind, D., G. A. Schmidt, J. Jonas, R. Miller, L. Nazarenko, M. Kelley, and J. Romanski, 2018:  
759 Multicentury instability of the Atlantic meridional circulation in rapid warming simulations with  
760 GISS ModelE2. *Journal of Geophysical Research: Atmospheres*, **123** (12), 6331–6355.

761 Rind, D., R. Suozzo, N. Balachandran, A. Lacis, and G. Russell, 1988: The GISS global climate-  
762 middle atmosphere model. Part I: Model structure and climatology. *Journal of the Atmospheric*  
763 *Sciences*, **45** (3), 329–370.

764 Rind, D., and Coauthors, 2020: GISS Model E2.2: A climate model optimized for the mid-  
765 dle atmosphere—model structure, climatology, variability, and climate sensitivity. *Journal of*  
766 *Geophysical Research: Atmospheres*, **125** (10), e2019JD032 204.

767 Roach, L. A., E. Blanchard-Wrigglesworth, S. Ragen, W. Cheng, K. C. Armour, and C. M. Bitz,  
768 2022: The impact of winds on AMOC in a fully-coupled climate model. *Geophysical Research*  
769 *Letters*, e2022GL101203.

770 Romanou, A., and Coauthors, Under Review: Stochastic bifurcation of the North Atlantic cir-  
771 culation under a mid-range future climate scenario with the NASA-GISS ModelE. *Journal of*  
772 *Climate*.



- 773 Shaw, T., and Coauthors, 2016: Storm track processes and the opposing influences of climate  
774 change. *Nature Geoscience*, **9** (9), 656–664.
- 775 Shaw, T. A., 2019: Mechanisms of future predicted changes in the zonal mean mid-latitude  
776 circulation. *Current Climate Change Reports*, **5** (4), 345–357.
- 777 Shepherd, T. G., 2014: Atmospheric circulation as a source of uncertainty in climate change  
778 projections. *Nature Geoscience*, **7** (10), 703–708.
- 779 Sigmond, M., and J. F. Scinocca, 2010: The influence of the basic state on the Northern Hemisphere  
780 circulation response to climate change. *Journal of Climate*, **23** (6), 1434–1446.
- 781 Simpson, I. R., T. A. Shaw, and R. Seager, 2014: A diagnosis of the seasonally and longitudinally  
782 varying midlatitude circulation response to global warming. *Journal of the Atmospheric Sciences*,  
783 **71** (7), 2489–2515.
- 784 Smith, D. M., and Coauthors, 2019: The polar amplification model intercomparison project  
785 (PAMIP) contribution to CMIP6: investigating the causes and consequences of polar amplifica-  
786 tion. *Geoscientific Model Development*, **12** (3), 1139–1164.
- 787 Swingedouw, D., P. Ortega, J. Mignot, E. Guilyardi, V. Masson-Delmotte, P. G. Butler, M. Khodri,  
788 and R. S  ferian, 2015: Bidecadal North Atlantic ocean circulation variability controlled by  
789 timing of volcanic eruptions. *Nature Communications*, **6** (1), 1–12.
- 790 Vallis, G. K., P. Zurita-Gotor, C. Cairns, and J. Kidston, 2015: Response of the large-scale structure  
791 of the atmosphere to global warming. *Quarterly Journal of the Royal Meteorological Society*,  
792 **141** (690), 1479–1501.
- 793 Visbeck, M., H. Cullen, G. Krahnmann, and N. Naik, 1998: An ocean model’s response to North  
794 Atlantic oscillation-like wind forcing. *Geophysical Research Letters*, **25** (24), 4521–4524.
- 795 Voigt, A., and T. A. Shaw, 2015: Circulation response to warming shaped by radiative changes of  
796 clouds and water vapour. *Nature Geoscience*, **8** (2), 102–106.
- 797 Yuval, J., and Y. Kaspi, 2020: Eddy activity response to global warming–like temperature changes.  
798 *Journal of Climate*, **33** (4), 1381–1404.

799 Zhai, H. L. J., Xiaoming, and D. P. Marshall, 2014: A simple model of the response of the Atlantic  
800 to the North Atlantic oscillation. *Journal of Climate*, **27** (11), 4052–4069.

801 Zhang, X., D. Waugh, and C. Orbe, Submitted: Response of Tropospheric Transport to Abrupt  
802 CO<sub>2</sub> Increase: Dependence on the Atlantic meridional overturning circulation. *Journal of Geo-*  
803 *physical Research: Atmospheres*.